비정질 셀레니움 박막의 결정화*

—결정의 형태와 그 변태속도—

김 기 순**

운모기판에 증착한 비정형 셀레니움 박막의 결정성장의 형태와 그 변태속도에 대하여 연구하였다. 열처리된 박막에서 비정질성분은 CS_2에 용해되나 결정질은 아무 변화없이 남아 있으므로 쉽게 현미경을 이용하여 그 모양을 조사할 수 있다. 결정은 (30°~100°C 온도 범위에서) 박막과 운모기판의 경계면을 따라서 원형상(구상 결정의 이차원 적 모양) 중심으로 부터 일정 속도로 자란다. 또한 필라멘트 형태의 결정이 원형상 결정의 비 규칙적인 부분에서 박막을 뚫고 위로 자란다. 이들 필라멘트형 결정은 자유표면에 도달하여 새로이 자유표면을 따라서 원형상으로 자라게 된다. 경계에 있는 원형상 결정의 두께는 약 500Å 정도이고 이것이 비정질 셀레니움 박막에서 보이는 "어두어 지는" 현상의 원인이 되고 있음이 밝혀졌다. 원형상 결정은 아주 조그마한 결정 "도메인"으로 구성되어 있으며 이들 "도메인"의 축 방향은 경계면과 나란하고 반경방향에 수직으로 되어 있다. 고온처리에서 일어지는 규칙적인 결정은 이들 "도메인"이 모이서 "라멜라"를 형성하여 중심부에서 부터 뻗어나가고 이들 "라멜라"간의 공간은 불규칙적으로 나열된 "도메인"으로 연결되어 있으며, 고분자 결정에 비하여 훨씬 두껍다. 반경 방향으로의 결정성장 속도는 아주 순도가 높은 박막에서는 시간에 따라 일정하고 주어진 온도에서 재현성이 아주 좋다. 이 실험에서 측정된 성장속도는 지금까지 발표된 이느 실험에서 관측된 것보다 빠르고 또 자유표면에서 자라는 속도에 비해서 약 백 여배나 빠르다. 결정 성장의 온도 의존은

$$u = 6 \times 10^{15} \exp\{-32.7(\text{kcal/mol})/RT\}\ \text{cm/sec}$$

로 표시할 수 있다.

1. INTRODUCTION

Dresner and Stringfellow[1] reported that the radial growth rates of spherulitic crystals in amorphous selenium films are sharply enhanced, by as much as an order of magnitude, by irradiation with light having wavelengths less than a critical value. They presented convincing evidence that this behavior reflects primarily the photo, rather than the thermal, effects of the irradiation. We decided to try to characterize these photo effects more fully. In the course of our study, we observed some important features of the pure thermal response of the morphology and kinetics of Se crystallization which seem to have escaped notice. In this paper we report these observations made on *a*-Se films of very high purity and comment on their implications to the crystallization mecha-

* 1973년 추기 총회에서 특별강연
J. Appl. Phys., Vol 44 No. 12, December 1973에 발표
** 한국 과학 기술연구소

nism as well as to the relation, considered by others,[2-4] of the crystallization morphology to that of linear polymers. We plan to report our results on the photo and impurity effects on crystallization in a future paper.

2. Experimental Procedures and Film Structure

The films were formed in a chamber evacuated to pressures less than 5×10^{-6} Torr by evaporating high purity selenium, nominal purity 99.999% (supplied by the Cerac/pure Co., Menomonee Falls, Wisconsin), from a tantalum boat onto freshly cleaved mica substrates held at room temperature. Deposition was carried out at rates of the order of 0.01—0.1μm/min to form amorphous films with thicknesses ranging between 0.05 and 20μm. We found that the as-formed films, as well as the amorphous parts of the films after partial crystallization, were completely dissolved by carbon disulfide after short times at room temperature. In contrast, the crystalline (hexagonal structure) parts of the film were left intact by the CS_2. This behavior facilitated examination of the crystallization morphology through the entire thickness of the film.

There is evidence that CS_2 selectively dissolves the ring components, primarily Se_8 molecules, of amorphous Se, leaving the chain component as residue[5]. From this we might infer, from their dissolution behavior, that our as-deposited films were composed almost entirely of molecules in ring forms. However, we have no other evidence to support this inference.

The extent and forms of the crystallization were investigated by optical and electron microscopy. A Reichert model MeF microscope was used for the optical observations. For convenience we shall, throughout the paper, refer to the various types of microscopic examination by combinations of the following symbols: I-interface, F-free surface, P-crossed polarizers, A-analyzer only, R-reflection, and T-transmission. For example, IPR will indicate an optical microscope observation on the mica-film interface side with crossed polarizers by reflected light. An AMR model 900 scanning electron microscope (SEM) was used to obtain micrographs of crystal surfaces exposed by CS_2 etches. The diffraction pattern and structure of some of the thin crystalline aggregates were examined by transmission electron microscopy (TEM) with a J. E. M. 120 electron microscope. Specimens for these observations were prepared by floating the crystallized films off the mica substrate by water immersion.

3. Results

A. Crystallization morphology

1 *General features*

Crystallization of the films occurred in the course of isothermal annealing, at temperatures ranging from 30 to 100°C, by the nucleation and growth of polycrystalline aggregates which

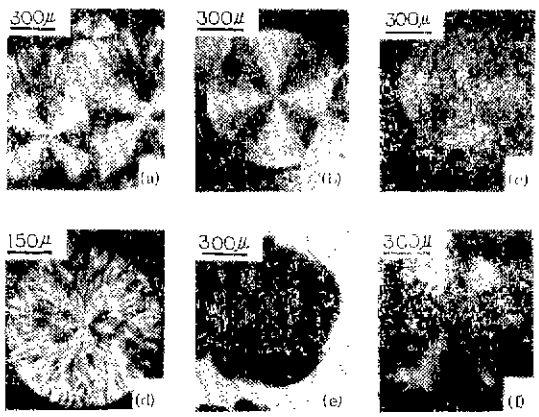

Fig. 1 Examples of various morphologies of interface cylindrites observed in different films. (a) (IPR) irregular, grown at room temperature during 6-month period; (b) (IPR) 100°C; (c) (IPR) 75°C; (d) (IPR) 67°C; (e) (FPR); and (f) (IPT) regular, 67°C

we shall call cylindrites. A cylindrite, the two-dimensional analog of spherulite, has a disklike form and is composed of crystallites radiating from the disk center, oriented so that the axes of their Se chains lie, approximately, in the disk plane perpendicular to a radial direction. The annealing was carried out by holding the specimens in an aluminum chamber, to be described in a future paper, at a controlled (±0.5°C) temperature.

All of the cylindrites observed appeared to have originated either at the mica-film interface (interface cylindrites, e.g., Fig. 1) or at the free surface (surface cylindrites). The interface cylindrites were examined most easily by polarized light, either reflected from the interface or transmitted through thin specimens. Surface cylindrites were observed by reflection of light from the free surface. Their radial growth rates were much less than those of the interface cylindrites; they were detected only after crystallization in the mica-film interfacial region was completed and in films which were much thicker than the thicknesses (approximately 500 Å) of the interface cylindrites. Often a surface cylindrite was found to connect to a filamentary crystal which seemed to have emanated from an interface cylindrite and grown through the film to the free surface.

2. *Interface cylindrites*

We noted that in the thicker films the interfacial region was completely crystallized by rapidly growing cylindrites before any free-surface crystallization was detected. In free-surface examinations this interfacial crystallization would not be apparent in films with thicknesses greater than 10–20μm, but in thinner films it is manifested by the well-knwn "visual darkening" and by reflection microscopy with polarized light, owing to the greater transmission of red light by the amorphous, relative to the crystalline, state of Se. Figure 1 shows the morphologies of some typical interface cylindrites as viewed from the interface side.

The thicknesses of the interface cylindrites, as measured by the Normanski technique, were found to be 500±100 Å and it appears that they remain essentially constant throughout most of the radial growth, though our evidence for this is not conclusive.

At a film thickness of the order of 500 Å the interface cylindrites can be observed from the free-surface side, and Fig. 2 shows some micrographs of such observations. Note that at its leading edge a cylindrite is much thinner than in its middle areas. Also, a small central region, the "double leaves" region [see Fig. 2 (d)] has remained amorphous. This region

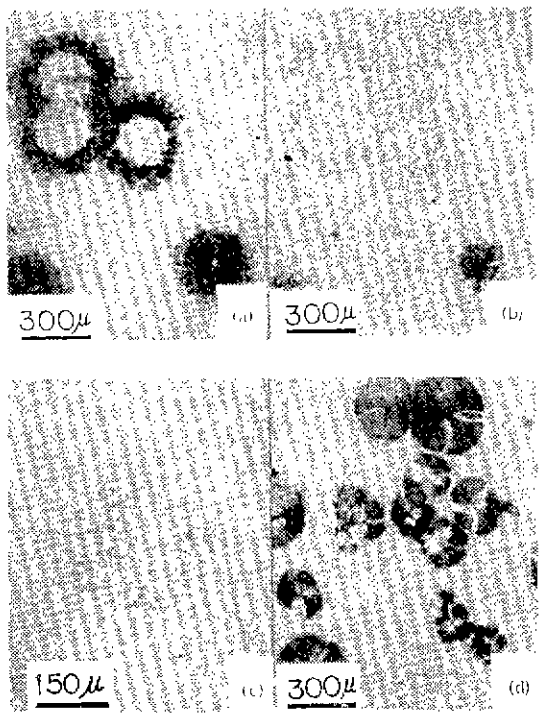

Fig. 2. Interface cylindrites growing in very thin films (approximately 500 Å thick) as viewed from free surface side. (a) (FPR) and (b) (FR), same specimen, 30 min at 77°C: (d) (FR), 17 min at 87°C; note apparently amorphous "double leaves" region.

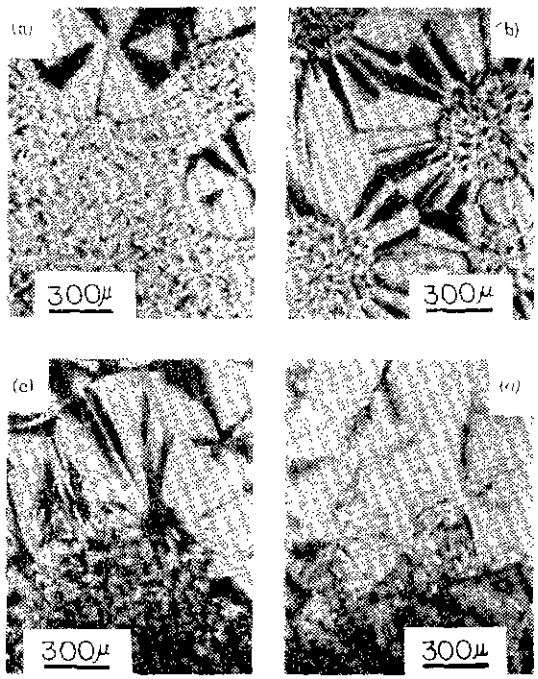

Fig. 3. Exhibitions of regular-and irregular-type morphologies within same specimens. All (IPR). (a) *Regular → irregular following growth temperature* change 100 → 72°C, (b) Irregular → regular due to upquench, 72 → 100°C. *(c) Rare simultaneous appe*arance of both types in nominally uniform film held *at 67°C for 90min (d) After long hold at 72°C;* mica substrate had been exposed to vapor from boiling water prior to film deposition.

crystallizes at a later stage to crystals with orientations very different from those which constitute the main body.

We note from Fig. 1 that the different cylindrites display quite different types of morphology, *ranging, from a* "regular" type seen in Figs. 1(e) and (f) to an "irregular" type as shown in Figs. 1(a)—(d). As we shall see, the degree of crystalline perfection is essentially higher in the regular than in the irregular cylindrites. *In general, the higher is the crys*tallization temperature, the more regular is the cylindrite morphology (see the sequence 1(a)—1(c) in Fig. 1). Apparently these morphologies are established in the course of crystallization and do not change detectably in subsequent annealing at temperatures as high as 100°C This behavior is most apparent from the results of temperature cycling experiments. For example, *Fig. 3(a) shows an abrupt change from a* regular to an irregular mode of growth accompanying the downquench, 100→72°C, and Fig. 3(b) shows the opposite change resulting from an upquench, 72→100°C.

The temperature at which the transition from the irregular to the regular morphology of growth is completed varies markedly with changes in the conditions, e.g., substrate preparation, of film deposition. For example, in some films the morphology is regular at crystallization temperatures as low as 57°C while in others it is quite irregular at crystallization temperatures as high as 100°C. Rarely, both regular and irregular morphologies are seen, as in Fig. 3 (c), in the same film following isothermal crystallization. Apparently the substrate preparation is quite a decisive factor, as may be seen from Fig. 3(d) which shows the crystallization morphology of a film deposited on a mica surface which had a prior exposure to vapor from boiling water. Also, we found that the growth temperature at which the morphology becomes regular is lowered by an increased substrate temperature (e.g., 40°C) during deposition, fast evacuation rate, slow evaporation, and formation of substrate by cleavage in dry nitrogen.

The microstructures of the interface cylindrites were examined by scanning electron microscopy (SEM) from both the free surface (see Fig. 4) and interface sides (see Fig. 5) of the film after the amorphous material had been dissolved away by CS_2. The crystallographic structure and orientations in the cylindrites were determined by the diffraction of transmitted electrons.

The scanning micrographs indicate that each cylindrite, whether regular or irregular, is co-

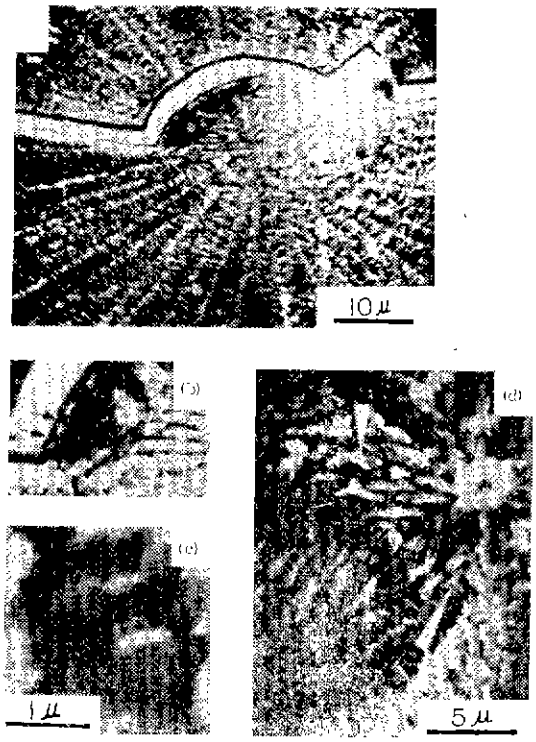

Fig. 4. Scanning electron micrographs (SEM's) of interface cylindrites on free-surface side after CS_2 etch (a) Note the crack due to etching, branching of lamella in region marked by rectangular frame. (b) Higher magnification of region near fracture; note (black arrows) that crack follows domain boundaries (c) Higher magnification of (a) remote from crack. (d) Central area of a different cylindrite; c axes are parallel with the longer dimension of domain; note (white arrows) that domain junctures are not invariably edge to edge or face to face.

mposed of small slablike crystallites, or domains, with thicknesses of the order of 0.1 μm and lateral dimensions of the order of 0.5—1 μm. Except in the "double leaves" region [see Fig. 4 (a)], the domains are always arranged in the cylindrite so that the c axes, which are parallel to the axes of the Se chains, lie in planes parallel to the substrate and in directions perpendicular to the radial directions of the cylindrite. The a axes exhibit no preferred orientations relative to the substrate plane. Figure 6 shows some of the diffraction patterns from regular cylindrites on which the analysis of orientation relations was based. The presence of forbidden spots in these patterns is attributed to double reflection.[6,7] In contrast with the arrangements in the main body of the cylindrite, the c axes in the central "double leaves" region are always more or less parallel to the boundary between the main body and the "double leaves". From this it appears that the direction along the longer dimensions of domains, as seen in Figs. 4(a) and 4(d), in regular cylindrites are parallel to the c axes

In the regular cylindrites most of the domains appear to be stacked together to form long arms or lamellae with irregular cross sections, which

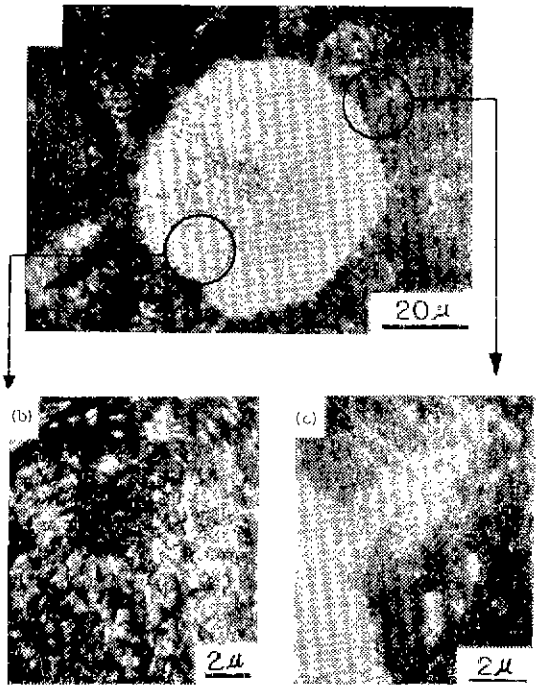

Fig. 5. SEM's of interface cylindrite on interface side after 1-h etch in CS_2. (a) Central region shows irregular growth at room temperature, outer region shows regular growth following upquench to 72°C. (b) Higher magnification of irregular region circled in (a); note both lateral and edgewise connection of domains. (c) Higher magnification of transition region circled in (a); note terraced layering on surface of regular cylindrite

extend radially from the central region to the edge and through the entire thickness of the cylindrite. Within a single lamella no differences in the orientations of adjacent domains were detected by diffraction, thus, the lamellar domain structure was apparent only from the CS_2 etch. The structure of these lamellae is somewhat similar to the "epitaxial lamellar overgrowths on intercrystalline links"[8] and the "shish-kebab" structures[9] sometimes observed in linear polymer systems. Between the lamellae there is a connective tissue consisting of a less dense aggregate of domains which are misoriented somewhat relative to the average and ideal orientation already specified. Note [Fig. 4(a)] the fracture which has formed parallel to an interlamellar boundary and the appearance of a new lamella in an interlamellar region well outside the central part of the cylindrite. It is the latter type of event which tends to keep the interlamellar spacing constant throughout the cylindrite growth.

As the crystallization temperature decreases, the grouping of domains into lamellae becomes less definite and, in what we have called irregular cylindrites, the lamellar structure is no longer apparent [see Figs. 5(a) and 5(b)]; in effect, the entire structure is the same as that of the interlamellar regions of the regular cylindrites. A transmission diffraction pattern from a portion of an irregular cylindrite is shown in Fig. 7(b) [cf pattern in Fig. 7(c) from a regular cylindrite]. It reflects a polycrystalline aggregate in the specified preferred orientation. The microstructures of an irregular (T_C=30°C) and regular (T_C=72°C) cylindrite, as viewed from the interface side, are compared directly in Fig. 5. We note that the individual domains, as indicated by the white spots, exhibit about the same size, despite the different crystallization temperatures. in both types of cylindrite. The structure, including the lamellae, of the regular cylindrite is not well defined on this micrograph owing to its resistance to etching.

3. *Comparison with morphology of linear polymer crystals*

It is apparent from the foregoing that the morphology of Se cylindrites differs in important respects from that of spherulites, as well as single crystals of organic linear polymers, even though the chain axes are for the most part similarly oriented in both types of structure. Most importantly the Se lamellae are very much thicker, by factors up to several hundred, and much more irregular in cross section than the lamellae formed in the crystallization of linear polymers. Even the length (500—5000Å)

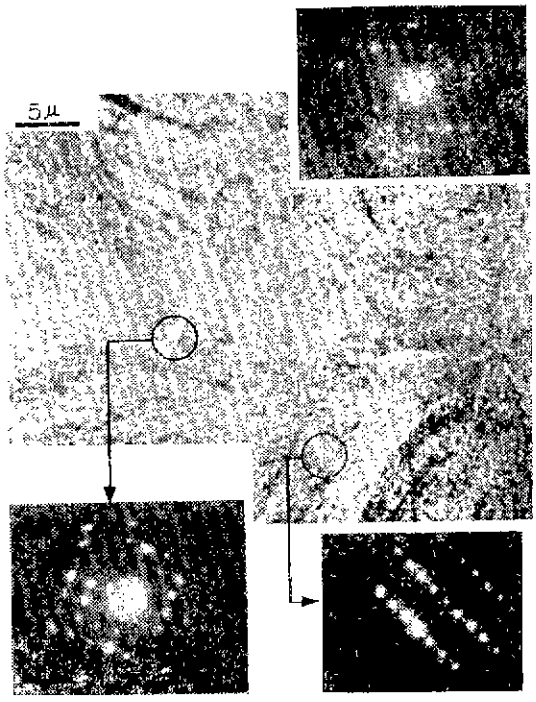

Fig. 6. Transmission electron micrograph (TEM) of central area of regular cylindrite and diffraction patterns, as corrected for image rotation, of selected areas. Directions of c axes are indicated by the longer diagonals of the white markers.

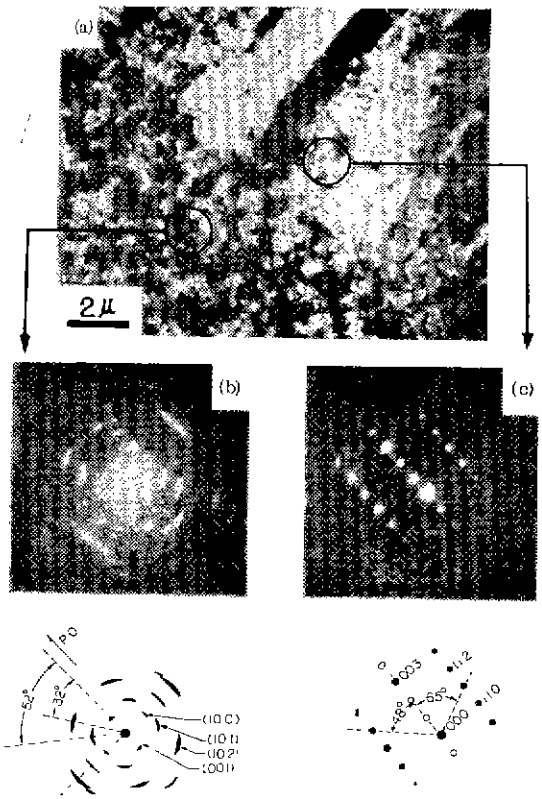

Fig. 7. TEM: (a) Boundary region between regular and irregular morphologies of a cylindrite. (b) Diffraction pattern, as corrected for image rotation, from an irregular region; arced rings indicate preferred orientation [001], relative to substrate plane and boundary direction. We assume that the (00.1) ring is due to double reflection. The axial ratio $c/a = 1.135$ was used for the analysis. (c) Single-crystal pattern from regular region; c axis is parallel to substrate plane and perpendicular to radial direction; double reflection spots are indicated by open circles.

of a single Se domain along the chain axis direction greatly exceeds the typical thicknesses of polymer lamellae. From this and the evidence from the dissolution behavior that the *a*-Se films are composed mainly of rings, it seems that chain folding is not essential for the Se crystal growth. Also, in contrast with the strong dependence of the polymer lamellae thicknesses on crystallization temperature T_C, the thicknesses of the Se domains seem not to vary systematically with T_C.

Still another unique feature of the Se cylindrite morphology is the occurrence in the central ("double leave") region of domains which appear to be oriented (see Figs. 4 and 5) with their chain axes far from the ideal direction (i.e., perpendicular to the radial direction) specified for the orientations in the outer part of the cylindrite. Indeed, some of the central domains seem to be oriented with their chain axes roughly parallel to a radial direction.

4. *Filamentary crystals*

We have noted that in the crystallization of the thicker films, filamentary crystals are sometimes generated by interface cylindrites and then grow through the film in isolated courses. Often free-surface cylindrites develop at the tips of these filaments after they have reached the suface.

Apparently the filaments originate only from the regions of the interface cylindrites the orientations of the domains deviate considerably from the specified ideal. In particular, they may stem from any part of an irregular cylindrite [Fig. 8 (a)], the central region of a regular cylindrite [Fig. 8 (c)], or from a boundary where two regular cylindrites have impinged on each other [Fig. 8(b)].

Frequently, the filaments start from irregular cylindritic regions at relatively low temperature but actually achieve most of their growth after the temperature is raised to the point where the morphology has changed to the regular type. When high-temperature growth of a cylindrite is interrupted periodically by cycling to and from room temperature, rings appear in the cylindrite which reflect narrow bands of irregular growth at room temperature. Many filaments stem from these rings and then grow rapidly in the high-temperature phases of the

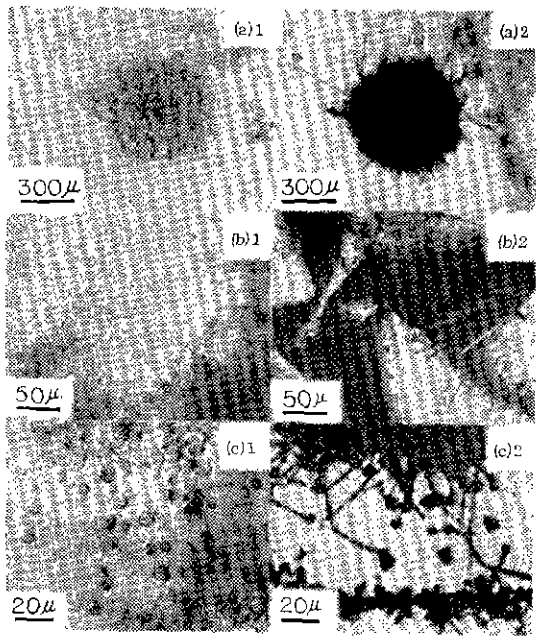

Fig. 8. Emergence of filamentary crystals in free surface and formation of surface cylindrites. Designations 1 and 2 distinguish reflection (FR) from transmission (FRT) micrographs of identical regions. (a) Filaments have grown 2 h at 72°C from irregular interface cylindrite formed during long period at room temperature. (b) Filaments stemming from interface of impingement of regular cylindrites on each other: 4h at 67°C. (c) Filaments emanating from central region of regular interface cylindrite after 8 h at 77 °C. Note that some filament ends have become centers of surface cylindrites.

cycle. This behavior is apparent from the micrographs shown in Fig. 9. The appearance of the rings is seen from the interface side in Fig. 9(a) and from the free-surface side, as manifested by the growing filaments, in Fig. 9(b). Figure 9(c) shows a SEM of the filaments from the free-surface side after their exposure by etching for 1 h in CS_2.

Figures 8(b1) (FR) and 8(b2) (FPT) clearly show the development of filaments from the impingement on each other of two regular cylindrties. The micrograph in Figure 8(b2) strongly suggests that the filaments are simply extensions of certain cylindrite lamellae. If so, we should expect to find that the crystallographic c axes are always perpendicular to the filament axes; thus, the direction of most rapid growth would be normal either to the (11.0) or (10.0) plane of the hexagonal crystal, We note, also, that the domain structure of filaments —exposed by CS_2 etching as in SEM. Figs. 10 (a) and 10(b), or just below the free surface as in SEM, Fig. 10(c)—is quite similar to that of the cylindrite lamellae.

Figures 8(c1) (FR) and 8(c2) (FPT) show filaments which have grown from the central

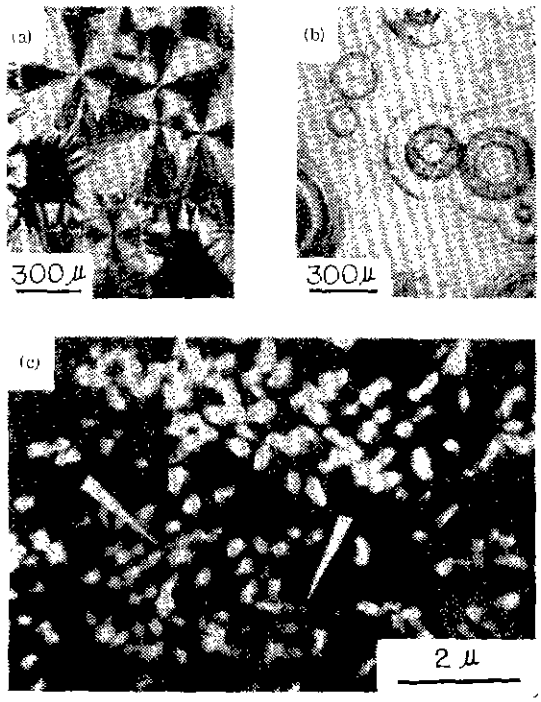

Fig. 9. Manifestation of filamentary crystals. (a) (IFR) Irregular central regions formed during 3 $\frac{1}{2}$ months at room temperature; outer regular regions of cylindrites formed in 2 min at 110°C (b) (FAR) different area of same specimen viewed from free surface. Filaments stemming from irregular regions of interface cylindrites are manifested by darkened areas. (c) (SEM) region of (b) viewed from free-surface side after 1-h etch in CS_2; this reveals filaments which formed rings in (b); arrows point to filaments which have joined laterally during growth.

region of a regular cylindrite. We note from the reflection micrographs, Figs. 8(a1)—8(c1), that surface cylindrites clearly have begun to develop from the ends of filaments which have reached the surface.

The foregoing observations strongly suggest that the filaments develop from certain domains in the interface cylindrites in orientations which deviate considerably from the specified ideal. That there is a considerable scatter of orientations about the irregular regions of the interface cylindrites is clear from the diffraction pattern (TEM), Fig. 7(b), from an irregular cylindrite. How the filamentary morphology is retained during growth is not clear. Possibly lateral growth or branching on the filament sidewalls is inhibited by a time-dependent impurity adsorption, in general accord with a model[10] proposed for the whisker morphology which develops in certain electrolytic growth processes.

Filaments growing side by side in close proximity often join together as may be seen in the micrograph, Fig. 9(c). Occasionally a filament splits and then the two parts rejoin at a later growth stage, as shown in Figs. 10(a) and 10(b). Also, it is interesting [see Fig. 10 (c)] that many of the filaments appear to grow more or less parallel to the free surface upon reaching its vicinity. It is not certain what the crystallographic orientation of the filament at this stage is. However, its faceting is similar to that of crystals which were shown[11,12] to be growing most rapidly in the direction of the *a* axis, so that the *c* axis would be perpendicular to the arrow tips.

5. *Surface cylindrites*

The occurrence of the transformation of filament tips, upon encountering the free surface,

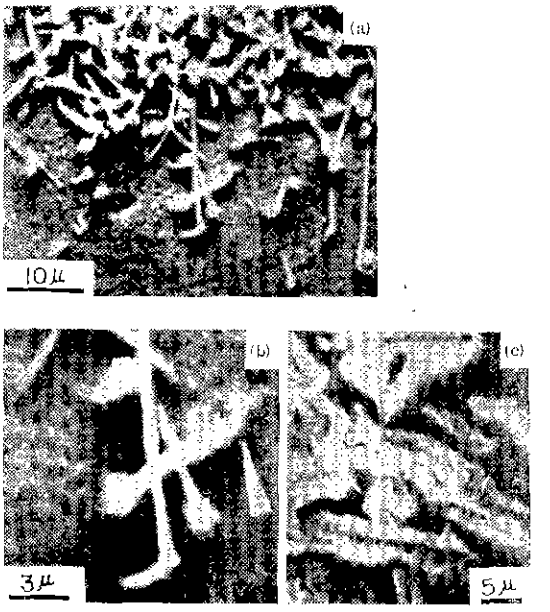

Fig. 10. SEM's of filamentary crystals. (a) Crystals from region similar to that in 8(c) exposed by 1-h etch in CS_2 (b) A more highly magnified region of (a) (c) No CS_2 etching; filaments in vicinity of free surface of different specimen after 5 min at 100 °C. Note (white arrow) apparent development of free-surface cylindrite.

into cylindrites is apparent from Fig. 8(b), which shows the tips in the free surface, in conjunction with Fig. 8(b), which shows a later stage of crystallization after cylindrites, clearly stemming from the filament tips, have developed. Figure 11(a) shows SEM's of filamentary tips and Figs. 11(b)—11(d) show surface cylindrites from different specimens. The dark bands around the cylindrite in Fig. 11(b) may reflect the rejection of impurities during growth.

The radial growth rates as well as the morphology of the surface cylindrites are quite sensitive to environmental conditions, such as humidity and illumination. Also, the growth rates are about two orders of magnitude less at the same temperature than those of the interface cylindrites.

It is evident from the foregoing that free-

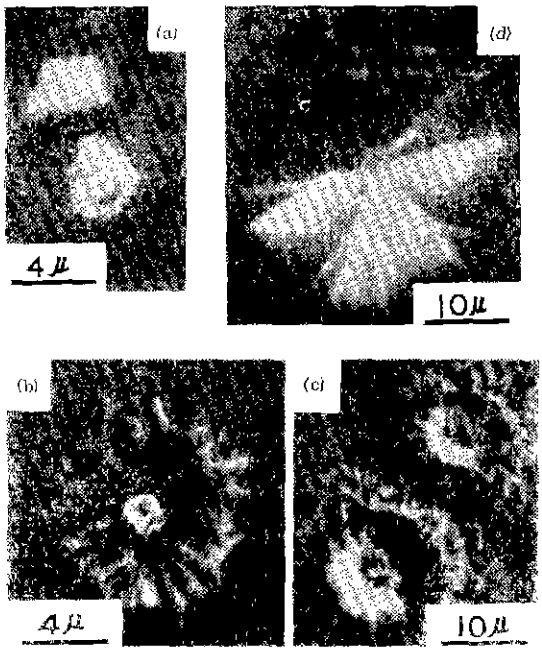

Fig. 11. SEM's showing morphology of free-surface cylindrites. Each micrograph is from a different specimen. Sequence (a)—(b) may show two stages of development. (b)—(d) show different modes of development.

surface observations alone may give an erroneous impression of the nature of cylindrite nucleation. For example, the apparently preferred nucleation in certain localized regions, seen in Fig. 8(b1), might have been attributed to film heterogrneities if the connection between free surface and interface cylindrites had not been established. Also, in films of intermediate thickness free surface cylindrites and the tops of interface cylindrites may occur simultaneously in the free surface, since crystallization preceeds much more rapidly at the interface than at the free surface.

B. Growth kinetics of interface cylindrites

The radial growth rates of the interface cylindrites were measured microscopically, either by continuous observation of samples on a temperature-controlled (±0.5°C) hot stage or by measurement of the separation of growth rings formed when growth at a high temperature was interrupted by cycling to and from room temperature. We have noted that these demarcation rings are made apparent by the irregular morphology and filament production of the small region grown at room temperature. Within experimental error the isothermal growth rate of any given cylindrite was found to be time independent.

The growth rates of the regular cylindrites

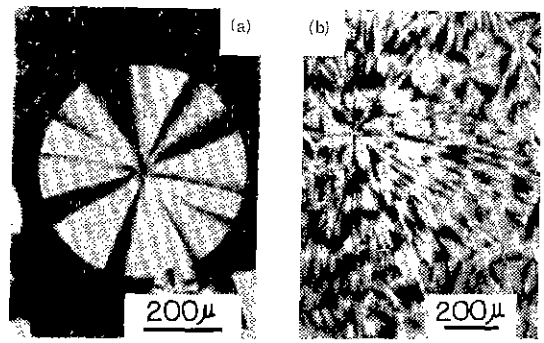

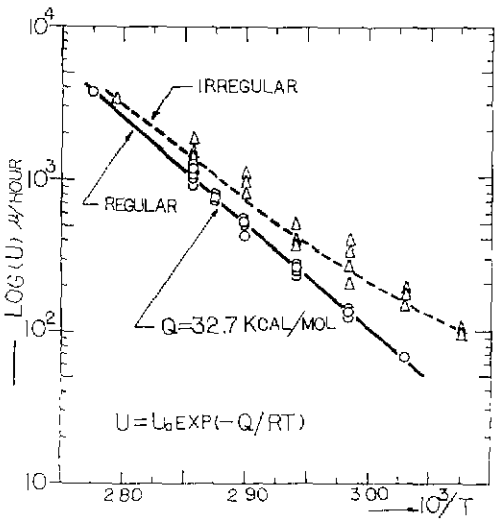

Fig. 12. Temperature dependence of radial growth rates of interface cylindrites. Micrographs show rings marking growth interruption by quench to room temperature (a) (IPR) regular cylindrite 67°C, growth intervals 40 min each. (b) (IPR) semiregular cylindrite, 77°C. growth intervals 10 min each.

were highly reproducible ($\pm 3\%$ for a given film and $\pm 10\%$ for different films) and their temperature dependence (see Fig. 12) was well characterized by an equation of the Arrhenius form:

$$u = 6 \times 10^{15} \exp\left(\frac{-32,700 \text{cal/mole}}{RT}\right) \text{cm/sec.}$$

In contrast, the growth rates of the irregular cylindrites (also see Fig. 8 for T dependence) scattered more and were considerably higher than those of the regular cylindrites. The differeerences between the growth rates of the two types of cylindrites decreases with increasing temperature, reflecting, perhaps, the increasing regularity of the morphology of the irregular cylindrite with increasing temperature. Our measured growth rates are almost two orders of magnitude higher than those reported by Crystal,[3] Keck,[13] and Hamada *et al.*[14] but are of the same order as those of Dresner and Stringfellow[1] with their most intense illumination. We made scattered observations on the radial growth rates of interface cylindrites in films deposited on glass or on KCl crystal surfaces formed by cleavage; these rates were substantially the same as those in the films deposited on mica. Also, the growth rates at lower temperatures were not appreciably changed by annealing the films at temperatures as high as high as 90°C.

The apparent activation energy for growth, 32.7kcal/mole, is of the order of the reported Se-Se bond energy, 41kcal/mole.[15] However, the preexponential factor is about 10^{10} times that which would be expected for a simple singly activated process:

$$\mu_o \fallingdotseq f\lambda\nu e^{\Delta S'/R},$$

where f is the fraction of surface sites which are *growth sites*, λ is the interatomic separation in radial direction, ν is the normal oscillation frequency of an atom or a segment of atoms in the amorphous-crystalline interfacial region, and $\Delta S'$ is the entropy of activation for growth. Also, we assume in the calculation that the thermodynamic driving free energy factor is at its maximum value, unity. The growth rates are of the magnitude of, though somewhat higher than, the values calculated from the scaling relation between growth rate and reciprocal viscosity. For these comparisons we used the melt viscosity data of Cukierman and Uhlmann[16], which may not be appropriate for vapor-deposited films.

The wide scatter in radial growth rates in different investigations, as well as between interface and free surface cylindrites, probably reflect, primarily, impurity effects. In covalent systems impurities can either catalyze or inhibit crystal growth. Our experience, to be described in a future paper, on the effects of addition of small concentrations of impurities, strongly suggsest that most of the variability in radial growth rates in deposited a-Se films is due to impurity inhibition effects.

IV. Discussion

Our observations have revealed a course of morphological evolution in crystallizing films of a-Se which seems not to have been recognized heretofore. There is the initial rapid growth of thin interface cylindrites to diameters as great as several millimeters. It is the formation of these cylindrites which accounts for the phenomenon of "visual darkening" of a-Se films. Filamentary crystals stem from the less regular parts of the interface cylindrites and grow through the films. Upon reaching the free surface the tips of some of these filaments generate cylindrites which grow in, and parallel to, the surface plane. Observation of this plane alone would have led

to the erroneous conclusion that each of these cylindrites had nucleated independently in the free-surface region. The mechanism whereby cylindrites are generated by the filamentary tips is still an unsolved problem.

It appears that the pattern of morphological development which we have outlined may be fairly general for *a*-Se films. Also, it may be the pattern followed in the crystallization of certain linear polymer thin films. More particularly, the two distinctly different types of spherulitic morphology reported for certain of these films[17,18] may reflect the simultaneous presence of interface and surface cylindrites.

We have noted that the molecular chain axes are perpendicular to the radial directions in the outer regions of both Se cylindrites and linear polymer spherulites. However, in view of the large dimensions of the individual domains, it does not seem likely that chain folding is required in the formation of Se cylindrites.

Acknowledgments

This research was supported in part by a grant from the office of Naval Research, Contract No. N00014-67-A-0298-0009. Also, some facilities provided by grants from the Advanced Research Projects Agency have been used. The authors are pleased to acknowledge the able assistance of G. R. Pierce in the electron microscopy studies and some helpful discussions with Professor D. R. Uhlmann of MIT on crystal morphology.

[1]J. Dresner and G. B. Stringfellow, J. Phys. Chem. Solids **29**, 303 (1968).

[2]B. Fitton and C. H. Griffiths, J. Appl. Phys. **39**, 3663(1968).

[3]R. C Crystal, J. Polymer Sci. A-2 **8**, 1755 (1970); **8**, 2153(1970).

[4]M C. Coughlin and B Wunderlich. Polym. Lett. **10**, 57(1972).

[5]J. Schottmiller, M. Tabak, G. Lucovsky, and A. Ward, J. Non-Cryst. Solids **4**, 80(1970).

[6]K. W Andrews. B. J. Dyson, and S. R Keown. *Interpretation of Electron Diffraction Patterns* (Plenum, New York, 1967), p. 52.

[7]C. H. Griffiths and H. Sang, Mater Res. Bull. **2**, 515(1967).

[8]H. D. Keith, F. J. Padden, Jr., and R. G. Vadimsky, J. Appl. Phys **37**, 4027(1966).

[9]A. J. Pennings, C J. H. Schouteten, and A. M. Kiel, J. Polymer Sci. C **38**, 167 (1970).

[10]P. B. Price, D A. Vermilyes, and M. B. Webb, Acta Metal. **6**, 524(1958)

[11]H. Ehinger, Z. Kristollgr. **115**, 235(1961).

[12]M. Shiojiri, Japan J. Appl. Phys. **6**, 163(1967).

[13]P. H. Keck, J. Opt. Soc Am. **42** 221(1952).

[14]S. Hamada, T. Sato, and T. Shirai, Bull. Chem. Soc. Japan **40**, 864(1967).

[15]A. Eisenberg and A. V. Tobolsky, J. Polym. Sci XLVI, 19(1960).

[16]M. Cukierman and D. R. Uhlmann (unpublished).

[17]See, for example, the micrograph of Fig. IV-40, p. 272 in P H. Geil, *Polymer Single Crystal* (Interscience, New York, 1963).

[18]F. J. Padden, Jr , H. D. Keith, N. M. Walter, and H. W. Wyckoff, J. Appl. Phys. **30**, 1485(1959).

「筆者紹介」

1963年 서울大學校工大原子力工學科卒業 金屬燃料研究所研究員. MIT 燃素工學科 博士過程을 마치고 Havard 大學 理工學部 研究員. 現在 KIST 素業材料室 研究員. 工學博士